Specific Interactions in Complexes Formed by DNA and Conducting Polymer Building Blocks: Guanine and 3,4-(Ethylenedioxy)thiophene

5 AUTHORS, INCLUDING:

Bruno Teixeira-Dias

iMICROQ (Integrated Microsystems for Quali…

14 PUBLICATIONS **83** CITATIONS

SEE PROFILE

Catherine Michaux

University of Namur

87 PUBLICATIONS **1,783** CITATIONS

SEE PROFILE

Eric A Perpète

University of Namur

173 PUBLICATIONS **6,006** CITATIONS

SEE PROFILE

Carlos Alemán

Polytechnic University of Catalonia

**462** PUBLICATIONS **6,004** CITATIONS

SEE PROFILE

ARTICLE

Specific Interactions in Complexes Formed by DNA and Conducting Polymer Building Blocks: Guanine and 3,4-(Ethylenedioxy)thiophene

Julien Preat,*,†,∥ Bruno Teixeira-Dias,‡,§ Catherine Michaux,†,⊥ Eric A. Perpète,†,# and Carlos Alemán*,‡,§

†Unité de Chimie Physique Théorique et Structurale, Facultes Universitaires Notre-Dame de La Paix, Rue de Bruxelles 61, 5000 Namur, Belgium

‡Departament d'Enginyeria Química, Higher Technical School for Industrial Engineering of Barcelona (ETSEIB), Universitat Politècnica de Catalunya, Av. Diagonal 647, Barcelona E-08028, Spain

§Center for Research in Nano-Engineering, Universitat Politècnica de Catalunya, Campus Sud, Edifici C', C/Pasqual i Vila s/n, Barcelona E-08028, Spain

Ⓢ *Supporting Information*

ABSTRACT: In the present paper we report direct experimental evidence of the existence of hydrogen bonds between poly(3,4-(ethylenedioxy)thiophene) (PEDOT) and DNA complexes and bring deeper knowledge about how such interactions can take place in such species. To this end, we used both experimental and theoretical methodologies to examine the interactions between the building blocks composing these two macromolecules. The specific interaction natures between 3,4-(ethylenedioxy)thiophene (EDOT, E) and doubly protonated guanine (GH_2^{2+}) monomers have been investigated using UV−vis spectroscopy. Quantum mechanical calculations in the density functional theory (DFT) and time-dependent density functional theory (TDDFT) frameworks have been used to identify the structures of the possible complexes. These differ in the interaction pattern, and it was possible to interpret the absorption spectra in terms of intermolecular interactions. Our results allow verification of the previous hypothesis about the formation of specific N−H···O interactions between G-containing nucleotide sequences and PEDOT. Clearly, DFT calculations indicate that E:GH_2^{2+} complexes are stabilized by N−H···O interactions, which involve an E oxygen and the −NH and −NH_2 moieties of GH_2^{2+}. Furthermore, TDDFT calculations are able to reproduce the absorption spectra (both energy gaps and relative oscillator strength magnitudes) of E and GH_2^{2+}, as well as the complex.
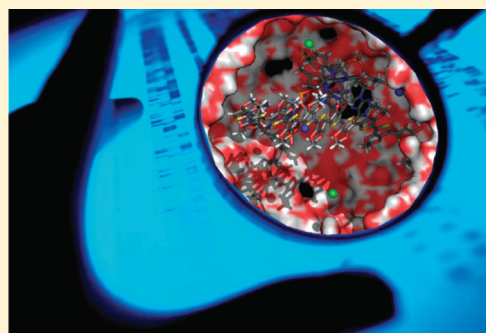
INTRODUCTION

The control of the interactions between π-conjugated polymers (π-CPs) and bioentities, such as living cells,[1,2] proteins,[3−7] or DNA,[8−13] is an essential research area for the development of advanced biotechnological applications. Within this context, we have been particularly interested in the recognition of nucleotide sequences using polypyrrole and polythiophene derivatives.[14−20] Precisely, we found that π-CPs bearing polar functional groups are able to act as hydrogen-bonding donors and/or acceptors and to form specific interactions with well-defined nucleotide sequences of plasmid DNA.[14−17] In contrast, associations between DNA and polymers without groups able to participate in hydrogen bonds, such as poly(3-methylthiophene) or polythiophene, were found to be nonspecific, although stable adducts can be detected.[5,16,18] These features evidenced that, among the specific interactions, hydrogen bonds are more important than other weak interactions (π−π stacking, hydrophobic, ...) in these systems.

The π-CPs we considered in this investigation are usually in a highly oxidized (doped) state.[14,16−19] Spontaneous interpolymer complexation between cationic polyelectrolytes and DNA is a well-known process, resulting from cooperative electrostatic forces.[21,22]

Accordingly, their unequivocal formation of electrostatic interactions between positively charged π-CPs and negatively charged DNA is expected to be essential for the formation and stability of the adducts. In a very recent study we have analyzed the influence of the doping level in the formation of specific interactions between DNA and π-CPs bearing polar functional groups.[19] Specifically, we considered a polymer in several oxidized states (1.0 and 0.5 positive charges per repeating unit) and in a reduced state (0.1 charge per repeating unit) states, and we proposed a mechanism for the formation of the adducts with DNA. That is an initial stabilization of the complexes thanks to nonspecific electrostatic interactions, followed by small structural rearrangements establishing specific hydrogen bonds between the polar groups of the π-CP and selected DNA bases. This process requires a structural alteration of the B-DNA double helix, which unfolds into two separated strands, as observed by circular dichroism and UV−vis spectroscopy.[17,19] The proposed mechanism we confirmed in a more recent investigation, in

Scheme 1. Molecular Structure of the PEDOT Unit
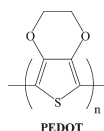
which the binding of an oxidized π-CP to a single-stranded DNA featuring the Dickerson dodecamer sequence was examined using molecular dynamics (MD) simulations.[21]

Among π-CPs, poly(3,4-(ethylenedioxy)thiophene), hereafter abbreviated PEDOT (Scheme 1), has attracted considerable interest due to a remarkable combination of properties such as low oxidation potential, good optical transparency, high conductivity (up to 500 S/cm), exceptional thermal and chemical stabilities, fast doping—undoping processes, and excellent biocompatibility.[23—27] Electrophoretic and spectroscopic studies on mixtures of plasmid DNA and oxidized or reduced PEDOT have shown the formation of stable adducts and of interactions with specific nucleotide sequences being confirmed through the protection imparted by this material against restriction enzymes.[16,18,19] Moreover, first-principle calculations using the MP2 quantum mechanical method indicated that the binding strength between the 3,4-(ethylenedioxy)thiophene (EDOT, E) monomeric units and DNA bases grows in the following order: adenine (A) < cytosine (C) < thymine (T) $\approx$ guanine (G).[18] These preferences were corroborated in a very recent MD study, in which the interaction between an oxidized PEDOT chain and a single DNA strand with sequence 5′-CGCGAATTCGCG-3′ has been inspected at the atomistic level.[20] These results unveiled the formation of specific O···H and S···H hydrogen bonds, $\pi-\pi$ stacking, and N—H···π interactions, in addition to the expected electrostatic interactions. In general, O···H hydrogen bonds were found to be very abundant and to have relatively large accumulated lifetimes, these specific interactions being more frequent with G and T than with A and C.

To get direct experimental evidence of the existence of hydrogen bonds between PEDOT and DNA, and to obtain more knowledge on how these interactions occur in such complexes, we here use a genuine combination of experimental and theoretical methodologies to investigate the interactions between the two macromolecule building blocks.

The specific interactions between E and G monomers have been investigated using UV—vis spectroscopy. Resorting to the density functional theory (DFT) and the time-dependent density functional theory (TDDFT) frameworks, we have identified structures of the possible E:G complexes, and we were able to interpret the absorption spectra in terms of intermolecular interactions. The results we obtained totally corroborate our previous hypothesis about the formation of specific N—H···O interactions between G-containing nucleotide sequences and PEDOT.

■ METHODS

Complexes. E and G were purchased from Aldrich and Sigma-Aldrich, respectively, while HCl and dimethyl sulfoxide (DMSO) of analytical reagent grade were purchased from Panreac. Trials with several solvents were performed to optimize the conditions for a complete solubilization of both E and G.

Initially, the two solutions were independently prepared: (i) 1 mg of G was dissolved in 1 mL of HCl (0.5 M, pH 0.3) to give

the protonated form GH_2^{2+} (see below), and (ii) 0.9 mg of E was dissolved in 1 mL of DMSO. Then a 1:1000 dilution was performed on each solution to obtain optimal concentrations for UV—vis spectroscopy assays. Complexes were formed in aqueous solution by mixing the diluted solutions of G in HCl and E in DMSO. Solutions were mixed to reach the following $E:GH_2^{2+}$ mass ratios: 0:1, 1:1, 1:2, 2:1, and 1:4. Final volumes were raised to 1 mL using mixed solutions of DMSO and HCl that were exactly prepared for each mass ratio. Obviously, the addition of HCl produces a very acidic environment, which is not the most appropriate situation for DNA in living species. However, G is relatively insoluble in neutral water, acidic environments being required for its complete solubilization. In spite of this limitation, it should be emphasized that the aim of this work is to provide details about the E:G interaction, which was proved to exist in PEDOT:DNA complexes solubilized in neutral water.[16,18,19,28]

Spectroscopic Studies. A UV-3600 (Shimadzu) UV—vis/NIR spectrophotometer controlled by the UVProbe V2.31 software was used to record UV—vis spectra of G, E, and E:GH_2^{2+} at room temperature in the 230—400 nm range, with a bandwidth of 2 mm, a scan speed of 600 nm/min, and a sampling interval of 0.1 nm. The deconvolution of the UV—vis spectra was performed using the PeakFit V4.0 software and applying a Gaussian deconvolution method with a width of 2 nm in full width at half-maximum (fwhm) mode and with a scan amplitude of 1.5%.

Computational Details. Calculations were performed with the Gaussian 09 package.[29] The geometry optimizations were performed in the solvent phase within the density functional theory framework at the B3LYP[30] level of theory with the 6-311G(d,p) basis set (BS).[31] The counterpoise method (CM) was used to correct the basis-set superposition error (BSSE) for the evaluation of the complexation driving force (ΔG) that was obtained through the computation of the infrared spectrum for each optimized structure, i.e., through the evaluation of the entropy. The binding energies (B) were calculated as the differences between the total internal energy of the optimized complex and the isolated monomers' internal energies associated with the complex equilibrium geometry. The vertical electronic excitations were obtained by using TDDFT[32—36] in the solvent-phase at the more refined CAM-B3LYP[37] level of theory with the large 6-311+G(2d,2p) BS.[31]

It is our experience that the combination of extended BSs with a long-range functional for TDDFT calculations is essential to accurately describe the electronic structures of systems likely to show marked charge-transfer excitations.[38,39]

The complexes were formed in DMSO, and the solvent effects on both the geometry optimizations and TDDFT calculations were taken into account by the polarizable continuum model (PCM).[40] In PCM, one usually divides the problem into a solute part (the complex) lying inside a cavity and a solvent part. By solving the Poisson equations at the interface, PCM gives a valid approximation of surrounding solvent effects. For the vertical excitation energies, we selected the so-called nonequilibrium PCM solutions.[41]

■ RESULTS AND DISCUSSION

G presents two positive pK_a values estimated at 3—4 and 9—10 in water.[42] In acidic solutions such as that of the present work, we have two sites that are protonated and the acidic form GH_2^{2+} is dominant, as depicted in Scheme 2. In the present

Scheme 2. Molecular Structure of GH_2^{2+} and the pK_a Values for the Two Protonated Sites of Interest
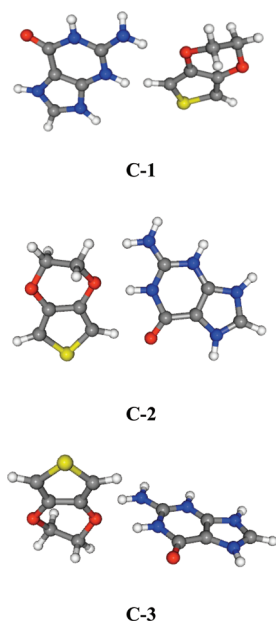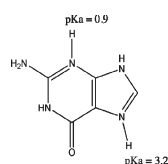

Figure 1. Molecular structures of the initial conformations of the three E:GH_2^{2+} complexes of interest (C-1, C-2, C-3).

Figure 2. Absorption (absorbance expressed with arbitrary units) spectra (black lines) of (a) EDOT, (b) GH_2^{2+}, and (c) E:GH_2^{2+} (1:1 mass ratio) determined in dilute solution (see the Methods). The curves and wavelength at the maxima resulting from the deconvolution process are also shown for each spectrum (gray lines).

study, we focused on three different E:GH_2^{2+} (1:1) complexes: C-1, C-2, and C-3 (Figure 1) have been chosen as starting conformations because it has been previously proved that their corresponding neutral forms (i.e., E:G complexes) show the best stability in both the gas and solvent phases.[18]

Figure 2 shows the absorption spectra recorded for diluted solutions of E, GH_2^{2+}, and E:GH_2^{2+} (1:1 mass ratio) with the curves resulting from the deconvolution process. Satisfactory statistical parameters (i.e., correlation coefficient $r^2 > 0.98$ and standard error (SE) <0.005) were obtained by considering two, two, and three isolated curves in the deconvolution of E, GH_2^{2+}, and E:GH_2^{2+} spectra, respectively.

As can be seen, diluted E presents two important transitions at 259 and 266 nm, while the GH_2^{2+} transitions are observed at 249 and 276 nm. For the complex, the deconvolution process led to three peaks centered on 247, 257, and 281 nm. It should be mentioned that the shoulder observed at the longest wavelength region precludes any reasonable fitting with a lower number of curves. Accordingly, the interactions between the two species, responsible for the formation of the complex, considerably affected one of the transitions. Although the peaks at 259 and 249 nm for E and GH_2^{2+}, respectively, undergo a change upon complexation (i.e., a 2 nm blue shift is detected), the peaks at 266 and 276 nm merge and red shift to 281 nm. Results obtained for complexes with 1:2, 2:1, and 1:4 mass ratios are very similar to those displayed in Figure 2c (data not shown). To interpret the
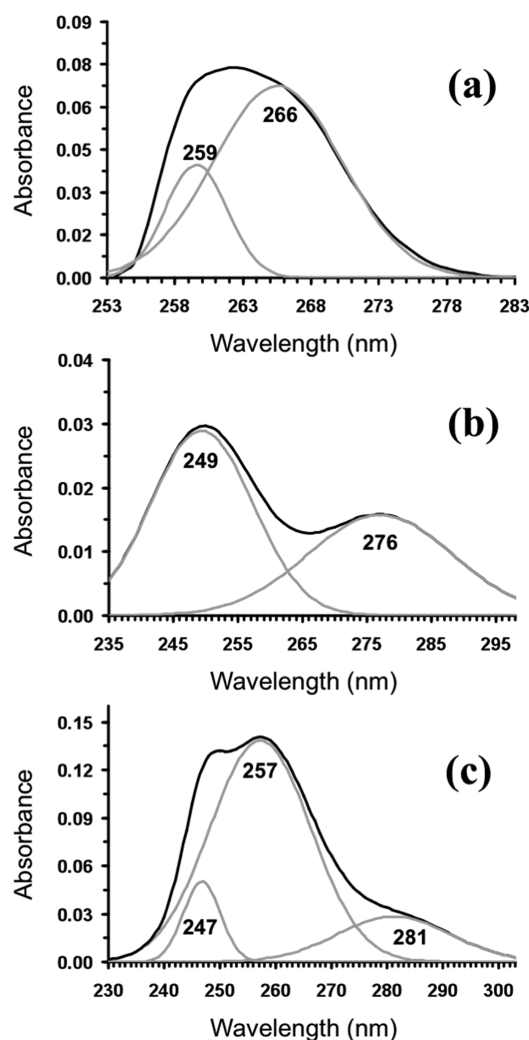
transitions depicted in Figure 2, quantum mechanical calculations were performed on E, GH_2^{2+}, and E:GH_2^{2+}.

Table 1 provides the binding energies and free enthalpies of complexation for the three above-evoked systems C-1, C-2, and C-3. All three systems present both binding energy and free enthalpy of complexation values of the same order of magnitude, that is, from 0.91 to 0.95 eV for B and from 0.25 to 0.28 eV for ΔG. This can be related to the fact that, for the three final structures, we have two H-bonds, implying an E oxygen and the $-NH^+$ and $-NH_2^+$ functions of GH_2^{2+}. Since C-2 and C-3

Table 1. Theoretical Binding Energies (B) and Free Enthalpies of Complexation (ΔG) (eV) for the Three G:E (1:1) Complexes in DMSO

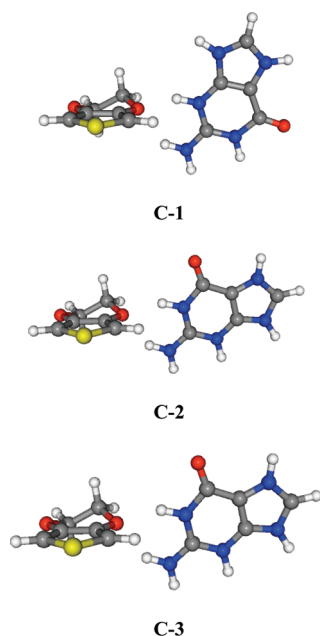| compound	B	ΔG
C-1	0.91	0.25
C-2	0.94	0.28
C-3	0.95	0.28

Figure 3. Molecular structures of the final conformations of the three E:GH_2^{2+} complexes of interest (C-1, C-2, C-3).

present similar structures after optimization, we compute equivalent B and ΔG values. However, the optimized E:GH_2^{2+} C-1 configuration is quite different with respect to C-2 and C-3 (Figure 3); i.e., the GH_2^{2+} carbonyl group is far from the guanine moiety, and this leads to an increase (a decrease) of the $-NH_2 \cdots O$ ($-NH \cdots O$) H-bond length.

The theoretical excitation energies for the GH_2^{2+}, E, C-1, C-2, and C-3 systems are listed and compared to the experimental data in Table 2. For all the considered systems, TDDFT systematically provides two peaks ($\lambda^{(1)}$, $\lambda^{(2)}$) in the high energetic region of the UV–vis spectrum.

For both GH_2^{2+} and E, the absorption band of lowest energy ($\lambda^{(1)}$) corresponds to a HOMO $\rightarrow$ LUMO transition. For GH_2^{2+}, the MOs depicted in Table 3 clearly show that $\lambda^{(1)}$ is related to an intramolecular charge transfer (CT) from the $-NH_2$ to the carbonyl, whereas for the second absorption band (HOMO $\rightarrow$ LUMO + 1 transition), the charge transfer occurs in the opposite direction (i.e., we have a $-C{=}O \rightarrow -NH_2$ photoinduced intramolecular CT). The nature of the CT is less obvious in the E case, but the MO analysis suggests that, for $\lambda^{(1)}$, the CT takes place from the oxygen atoms in the heterocycle to the aromatic moiety (the MO is mainly localized on the C–H bond), whereas for $\lambda^{(1)}$ we have a HOMO $-$ 1 $\rightarrow$ LUMO CT from the oxygen atoms to the sulfur atom.

Concerning the complexes, Table 3 reveals the intermolecular nature of the CT involved in the first excitation. Clearly, the HOMO $\rightarrow$ LUMO + 4 transition is predominantly localized on E, with a slight contribution from both the $-NH_2$ and NH functions of GH_2^{2+} (LUMO + 4). On the contrary, $\lambda^{(2)}$ is characterized by a pure intramolecular CT localized on the protonated guanine, and the topology nature of the C-1 $\lambda^{(2)}$ MOs is similar to that observed for the first excitation of isolated GH_2^{2+}, i.e., a $-NH_2 \rightarrow -C{=}O$ photoinduced intramolecular CT. The similarity between the MOs involved in the GH_2^{2+} HOMO $\rightarrow$ LUMO transition and in the C-1 HOMO $-$ 2 $\rightarrow$ LUMO transition can explain the similar excitation energies and

oscillator strengths computed for GH_2^{2+} $\lambda^{(1)}$ (5.37 eV, $f = 0.22$) and C-1, C-2, and C-3 $\lambda^{(2)}$ (5.32 and 5.7 eV, $f = 0.17$ and 0.21).

To refine the analysis of the MO topology involved in the CT transitions, the natural transition orbital (NTO) formalism has been employed to analyze our results. This has been done by using the Nancy_Ex software, a program recently developed by Assfeld's group.[43] The molecular orbitals from the NTO treatment are depicted in Table SI.1 (Supporting Information). For each transition ($\lambda^{(1)}$ and $\lambda^{(2)}$), the NTO provides the hole (H) and electron (Elec) redistribution. Thus, $|H|^2$ physically represents the amount of electron density that is removed from the ground state during the excitation, whereas $|Elec|^2$ represents the density that is rearranged on the excited state. Therefore, the transition can be represented by means of a passage from $|H|^2$ to $|Elect|^2$. A comparison between the NTO procedure (Table SI.1) and the more conventional DFT-MO analysis (Table 3) lets us conclude that (i) for GH_2^{2+} and E, both the DFT-MO and NTO analyses provide the same trends (i.e., the conventional and the NTO MOs are similar), (ii) for C-1, the HOMO $\rightarrow$ LUMO + 4 and the H($\lambda^{(1)}$) $\rightarrow$ Elec($\lambda^{(1)}$) imply MOs presenting similar topologies with a transition that is predominantly localized on E, with a slight contribution from GH_2^{2+}, and (iii) on the contrary, the NTO underlines a strong intermolecular CT character for $\lambda^{(2)}$ whereas the conventional HOMO $-$ 2 $\rightarrow$ LUMO a pure intramolecular CT localized on the protonated guanine. Clearly, for the second transition computed at 5.32 eV, the amount of electron density that is removed from the ground state during the excitation is also localized on the EDOT moiety.

Without a doubt, although the MOs involved in an intramolecular CT are well described through both the NTO and conventional approaches, the last one fails to correctly reproduce the MO topology for long-range CT. Therefore, we strongly recommend the NTO as an approach for the accurate description of the MOs involved in long-distance CT.
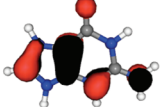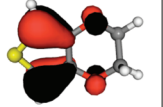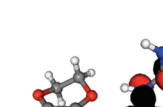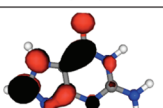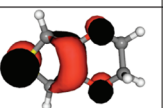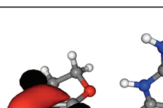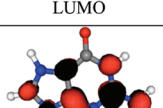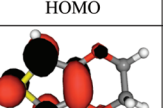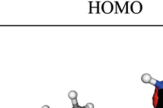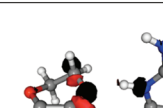
For GH_2^{2+} and E, our TDDFT procedure correctly reproduces the $\lambda^{(1)}-\lambda^{(2)}$ energy gap (Δ) as well as the relative $\lambda^{(1)}-\lambda^{(2)}$ oscillator strength magnitude. Indeed, the computed Δ values are 0.46 and 0.16 eV for GH_2^{2+} and E, respectively, whereas these gaps are measured at 0.49 and 0.12 eV. On the other hand, the relative $f^{(1)}/f^{(2)}$ parameter is estimated at 0.63 and 2.40 for GH_2^{2+} and E, respectively. These values are in qualitative agreement with the experimental trends. Indeed, for E we have peaks at 259 and 266 nm with an absorbance ratio $f^{(1)}/f^{(2)}$ of 0.57, whereas for GH_2^{2+}, it is 1.84 with peaks at 249 and 276 nm ($f^{(1)}/f^{(2)} = 0.029/0.016$). While the theory successfully characterizes the UV–vis spectra of both the isolated GH_2^{2+} and EDOT, the analysis of the TDDFT results is tricky for the complexed species. Indeed, whereas two absorption bands are predicted by TDDFT, the deconvolution reveals three peaks at 4.41, 4.82, and 5.02 eV (281, 257, and 247 nm, respectively). Obviously, as a characteristic feature, the absorption spectrum of the E:GH_2^{2+} complex presents several maxima in the short-wave band. Though many hypotheses can be held to elucidate such spectral patterns, a vibrational coupling is the most probable as the distance between the two neighboring peaks at 257 and 247 nm sticks to the well-defined IR frequency, $1600-1700$ cm^{-1} stretching frequencies of carbonyl or ethylene side groups, which actually correspond to 0.20 eV separation experimentally observed for the complex. Note that the gap between the peaks at 281 and 247 nm is larger than 0.60 eV. This is equivalent to a 5000 cm^{-1} separation, obviously out of the infrared region. The IR spectrum for C-1 clearly shows an absorption band of high intensity at 1720 cm^{-1} matching

Table 2. Comparison between Experimental and Theoretical UV–Vis Absorption Bands, λ (eV [nm]), for the Doubly Protonated Guanine (GH_2^{2+}), EDOT (E), and the C-1, C-2, and C-3 Complexes (1:1) in DMSO[a]

| | experiment | | theory (f) | |
compound	$\lambda^{(1)}, \lambda^{(2)}$	Δ	$\lambda^{(1)}, \lambda^{(2)}$	Δ
GH_2^{2+}	4.49, 4.98 [276, 249]	0.49 [27]	5.37 (0.22), 5.83 (0.35) [231, 213]	0.46 [18]
E	4.66, 4.78 [266, 259]	0.12 [7]	5.23 (0.24), 5.39 (0.10) [237, 230]	0.16 [7]
C-1	4.41, 4.82, 5.02 [281, 257, 247]	0.41 [24]	5.26 (0.24), 5.32 (0.17) [236, 233]	0.06 [3]
C-2			5.26 (0.24), 5.37 (0.21) [236, 231]	0.11 [5]
C-3			5.26 (0.24), 5.37 (0.21) [236, 231]	11 [5]

compound	MO label ($\lambda^{(1)}, \lambda^{(2)}$)
GH_2^{2+}	HOMO → LUMO, HOMO → LUMO + 1
E	HOMO → LUMO, HOMO − 1 → LUMO
C-1	HOMO → LUMO + 4, HOMO − 2 → LUMO
C-2	HOMO → LUMO + 4, HOMO − 2 → LUMO
C-3	HOMO → LUMO + 4, HOMO − 2 → LUMO

[a] Δ is the absolute energy difference between the first and second excitations (eV [nm]). We also provide the oscillator strength f related to the theoretical $\lambda^{(1)}$ and $\lambda^{(2)}$ and the related molecular orbital (MO) labels.

Table 3. Graphical Representation of the MOs (and Their Labels) Involved in $\lambda^{(1)}$ and $\lambda^{(2)}$ for GH_2^{2+}, E, and C-1 Obtained at the PCM(DMSO)-B3LYP/6-311G(d,p) Level of Theory with a Contour Threshold Fixed at 0.05 |e|

GH_2^{2+}	E	C-1
HOMO	HOMO-1	HOMO-2
LUMO	HOMO	HOMO
LUMO+1	LUMO	LUMO
		LUMO+4

not taken into account in theory, and therefore, its effects are not computed. Thus, the deficiencies mentioned above for the complex have been attributed to such a limitation.

These results confirm that G and H interact with specific N−H···O secondary bonds. It should be noted that, although the existence of weak hydrogen-bonding interactions was proposed in previous studies describing PEDOT:DNA complexes,[16,18−20,28] no direct experimental evidence of their existence was obtained. As a result, the fast formation of PEDOT:DNA adducts could be governed by electrostatic attraction between the positively charged polymer molecules (a +0.5 |e| per repeating unit was measured[25] for the oxidized PEDOT) and the negatively charged phosphate groups of DNA. However, the presence of weak interactions with specific nucleotide sequences was postulated as an explanation of both the protection imparted by PEDOT to DNA digestion in the presence of selected restriction enzymes[16,18,19] and the formation of stable complexes when the charge of PEDOT was electrochemically reduced from +0.5 to +0.1 |e| per repeating unit.[19] In this work, strong electrostatic interactions are not possible due to the lack of both negatively charged phosphate groups and oxidized EDOT units. The DFT calculations presented here show that the building blocks can form complexes stabilized through specific N−H···O interactions. The agreement between the experimental and calculated absorption spectra highlights the crucial role played by these interactions in PEDOT:DNA complexes.

■ CONCLUSIONS

In this work we used UV–vis spectroscopy and quantum mechanical tools to examine the specific interactions in complexes formed between GH_2^{2+} and EDOT, which can be considered as building blocks of plasmid DNA and PEDOT, respectively. To prepare E:GH_2^{2+} mixtures with mass ratios of 1:1, 1:2, 2:1, and 1:4, an acidic pH was required, which leads to the protonation of G. Nevertheless, E:GH_2^{2+} can be considered as a reliable model compound since the coexistence of negatively charged phosphate groups in DNA and the positive charges of the oxidized polymer is avoided.

with the stretching of the GH_2^{2+} carbonyl. In such a context, we can associate the second excitation with the experimental UV–vis peak that presents the highest intensity after deconvolution, i.e., the band at 257 nm (4.82 eV). It should be noted that the vibrational coupling, which may enhance the oscillator strengths of the first two transitions, is present in the experimental spectrum, even though it is

DFT calculations indicate that E:GH$_2^{2+}$ complexes are stabilized by N−H···O interactions involving an E oxygen and the −NH and −NH$_2$ moieties of GH$_2^{2+}$. Furthermore, TDDFT calculations reproduce the absorption spectra (both energy gaps and relative oscillator strength magnitudes), not only for E and GH$_2^{2+}$ but also for the complex. In summary, these results provide clear evidence of the existence of specific N−H···O interactions in the systems studied here, allowing confirmaton of the previous mechanistic hypothesis explaining the former experimental observations.

■ ASSOCIATED CONTENT

ⓢ **Supporting Information.** Graphical representation of the molecular orbitals from the NTO treatment for GH$_2^{2+}$, E, and C-1. This material is available free of charge via the Internet at http://pubs.acs.org.

■ AUTHOR INFORMATION

Corresponding Authors
*E-mail: julien.preat@fundp.ac.be (J.P.); carlos.aleman@upc.edu (C.A.).

Notes
$^{\parallel}$Postdoctoral research associate of the Belgian Fund for Scientific Research (FNRS).
$^{\perp}$Research associate of the FNRS.
$^{\#}$Senior research associate of the FNRS.

■ ACKNOWLEDGMENT

■ REFERENCES

(1) Lee, J. W.; Serna, F.; Nickels, J.; Schmidt, C. E. *Biomacromolecules* **2006**, *7*, 1692–1695.
(2) del Valle, L. J.; Estrany, F.; Armelin, E.; Oliver, R.; Alemán, C. *Macromol. Biosci.* **2008**, *8*, 1144–1151.
(3) Azioune, A.; Chehimi, M. M.; Miksa, B.; Basinska, T.; Slomkowski, S. *Langmuir* **2002**, *18*, 1150–1156.
(4) Sanghvi, A. B.; Miller, K. P. H.; Belcher, A. M.; Schmidt, C. E. *Nat. Mater.* **2005**, *4*, 496–502.
(5) Peng, H.; Zhang, L.; Spires, J.; Soeller, C.; Travas-Sejdic, J. *Polymer* **2007**, *48*, 3413–3419.
(6) Fan, Y.; Chen, X. T.; Trigg, A. D.; Tung, C. H.; Kong, J. M.; Gao, Z. Q. *J. Am. Chem. Soc.* **2007**, *129*, 5437–5443.

(7) Dawn, A.; Nandi, A. K. *Macromolecules* **2005**, *38*, 10067–10073.
(8) Xu, Q. H.; Gaylord, B. S.; Wang, S.; Bazan, G. C.; Moses, D.; Heeger, A. J. *Proc. Natl. Acad. Sci. U.S.A.* **2004**, *101*, 11634–11639.
(9) Xu, Q. H.; Wang, S.; Korystov, D.; Mikhailovsky, A.; Bazan, G. C.; Moses, D.; Heeger, A. J. *Proc. Natl. Acad. Sci. U.S.A.* **2005**, *102*, 530–535.
(10) Gaylord, B. S.; Heeger, A. J.; Bazan, G. C. *J. Am. Chem. Soc.* **2003**, *125*, 896–900.
(11) Wang, S.; Liu, B.; Gaylord, B. S.; Bazan, G. C. *Adv. Funct. Mater.* **2003**, *13*, 463–467.
(12) Xia, F.; Xiaolei, Z.; Yang, R.; Xiao, Y.; Kang, D.; Vallée-Bélise, A.; Gong, X.; Heeger, A. J.; Plaxco, K. V. *J. Am. Chem. Soc.* **2010**, *132*, 1252–1254.
(13) Kim, Y.; Whitten, J. E.; Swager, T. M. *J. Am. Chem. Soc.* **2005**, *127*, 12122–12130.
(14) Pfeiffer, P.; Armelin, E.; Estrany, F.; del Valle, L. J.; Cho, L. Y.; Alemán, C. *J. Polym. Res.* **2008**, *15*, 225–234.
(15) Zanuy, D.; Alemán, C. *J. Phys. Chem. B* **2008**, *112*, 3222–3230.
(16) Ocampo, C.; Armelin, E.; Estrany, F.; del Valle, L. J.; Oliver, R.; Sepulcre, F.; Alemán, C. *Macromol. Mater. Eng.* **2007**, *292*, 85–94.
(17) Teixeira-Dias, B.; del Valle, L. J.; Estrany, F.; Armelin, E.; Oliver, R.; Alemán, C. *Eur. Polym. J.* **2008**, *44*, 3700–3707.
(18) Alemán, C.; Teixeira-Dias, B.; Zanuy, D.; Estrany, F.; Armelin, E.; del Valle, L. J. *Polymer* **2009**, *50*, 1965–1974.
(19) Teixeira-Dias, B.; Zanuy, D.; del Valle, L. J.; Estrany, F.; Armelin, E.; Alemán, C. *Macromol. Chem. Phys.* **2010**, *211*, 1117–1126.
(20) Preat, J.; Zanuy, D.; Perpète, E. A.; Alemán, C. *Biomacromolecules* **2011**, *12*, 1298.
(21) Kircheis, R.; Blessing, T.; Brunner, S.; Wightman, L.; Wagner, E. *J. Controlled Release* **2001**, *7*, 165–170.
(22) Wolfert, M. A.; Dash, P. R.; Navarova, O.; Oupicky, D.; Seymour, L. W.; Smart, S.; Strohalm, J.; Ulbrich, K. M. A. *Bioconjugate Chem.* **1999**, *10*, 993–1004.
(23) Heywang, G.; Jonas, F. *Adv. Mater.* **1992**, *4*, 116.
(24) Dietrich, M.; Heinze, J.; Heywang, G.; Jonas, F. *J. Electroanal. Chem.* **1994**, *369*, 87.
(25) Ocampo, C.; Oliver, R.; Armelin, E.; Alemán, C.; Estrany, F. *J. Polym. Res.* **2006**, *13*, 193.
(26) Tamburri, E.; Orlanducci, S.; Toschi, F.; Terranova, M. L.; Passeri, D. *Synth. Met.* **2009**, *159*, 406.
(27) del Valle, L. J.; Aradilla, D.; Oliver, R.; Sepulcre, F.; Gamez, A.; Armelin, E.; Alemán, C.; Estrany, F. *Eur. Polym. J.* **2007**, *43*, 2342.
(28) Teixeria-Dias, B.; Zanuy, D.; Poater, J.; Sola, M.; Estrany, F.; Del Valle, L. J.; Alemán, C. *Soft Matter* **2011**, *7*, 9922–9932.
(29) Frisch, M. J.; Trucks, G. W.; Schlegel, H. B.; Scuseria, G. E.; Robb, M. A.; Cheeseman, J. R.; Scalmani, G.; Barone, V.; Mennucci, B.; Petersson, G. A.; Nakatsuji, H.; Caricato, M.; Li, X.; Hratchian, H. P.; Izmaylov, A. F.; Bloino, J.; Zheng, G.; Sonnenberg, J. L.; Hada, M.; Ehara, M.; Toyota, K.; Fukuda, R.; Hasegawa, J.; Ishida, M.; Nakajima, T.; Honda, Y.; Kitao, O.; Nakai, H.; Vreven, T.; Montgomery, Jr., J. A.; Peralta, J. E.; Ogliaro, F.; Bearpark, M.; Heyd, J. J.; Brothers, E.; Kudin, K. N.; Staroverov, V. N.; Kobayashi, R.; Normand, J.; Raghavachari, K.; Rendell, A.; Burant, J. C.; Iyengar, S. S.; Tomasi, J.; Cossi, M.; Rega, N.; Millam, N. J.; Klene, M.; Knox, J. E.; Cross, J. B.; Bakken, V.; Adamo, C.; Jaramillo, J.; Gomperts, R.; Stratmann, R. E.; Yazyev, O.; Austin, A. J.; Cammi, R.; Pomelli, C.; Ochterski, J. W.; Martin, R. L.; Morokuma, K.; Zakrzewski, V. G.; Voth, G. A.; Salvador, P.; Dannenberg, J. J.; Dapprich, S.; Daniels, A. D.; Farkas, Ö.; Foresman, J. B.; Ortiz, J. V.; Cioslowski, J.; Fox, D. J. *Gaussian 09*, revision A.1; Gaussian, Inc.: Wallingford, CT, 2009.
(30) Becke, A. D. *J. Chem. Phys.* **1993**, *98*, 5648.
(31) Frish, M. J.; Pople, J. A.; Binkley, J. S. *J. Chem. Phys.* **1984**, *80*, 3265.
(32) Preat, J.; Michaux, C.; Lewalle, A.; Perpète, E. A.; Jacquemin, D. *Chem. Phys. Lett.* **2008**, *451*, 37.
(33) Preat, J.; Loos, P. F.; Assfeld, X.; Jacquemin, D.; Perpète, E. A. *Int. J. Quantum Chem.* **2007**, *107*, 574.
(34) Preat, J.; Jacquemin, D.; Wathelet, V.; André, J. M.; Perpète, E. A. *Chem. Phys.* **2007**, *335*, 177.

(35) Furche, F.; Ahlrichs, R. *J. Chem. Phys.* **2002**, *117*, 7433.

(36) Scalmani, G.; Frisch, M. J.; Mennucci, B.; Tomasi, J.; Cammi, R.; Barone, V. *J. Chem. Phys.* **2006**, *124*, 094107.

(37) Yanai, T.; Tew, D.; Handy, N. *Chem. Phys. Lett.* **2004**, *393*, 51.

(38) Preat, J. *J. Phys. Chem. C* **2010**, *114*, 16716.

(39) Jacquemin, D.; Preat, J.; Perpète, E. A. *Chem. Phys. Lett.* **2005**, *410*, 254.

(40) Tomasi, J.; Mennucci, B.; Cammi, R. *Chem. Rev.* **2005**, *105*, 2999.

(41) Cossi, M.; Barone, V. *J. Chem. Phys.* **2001**, *115*, 4708.

(42) Jang, Y. H.; Goddard, W. A., III; Noyes, K. T.; Sowers, L. C.; Hwang, S.; Chung, D. S. *J. Phys. Chem. B* **2003**, *107*, 344.

(43) *NAncy EX:* Project Web Hosting - Open Source Software. http://nancyex.sourceforge.net.